Angewandte Chemie
Eine Zeitschrift der Gesellschaft Deutscher Chemiker

Supporting Information

Electrochemiluminescence Enhanced by a Non-Emissive Dual Redox Mediator

N. S. Adamson, S. J. Blom, E. H. Doeven, T. U. Connell, C. Hadden, S. Knežević, N. Sojic, A. Fracassa, G. Valenti, F. Paolucci, J. Ding, Y. Wang, B. Su*, C. Hua, P. S. Francis**

Supplementary Information for:

Electrochemiluminescence Enhanced by a Non-Emissive Dual Redox Mediator

Natasha S. Adamson,[a,†] Steven J. Blom,[a,†] Egan H. Doeven,[a] Timothy U. Connell,*[,a] Callum Hadden,[a] Sara Knezevic,[b] Neso Sojic,[b] Alessandro Fracassa,[c] Giovanni Valenti,[c] Francesco Paolucci,[c] Jialian Ding,[d] Yafeng Wang,[d] Bin Su,*[,d] Carol Hua,[e] Paul S. Francis*[,a]

[a]Centre for Sustainable Bioproducts, Faculty of Science, Engineering and Built Environment, Deakin University, Geelong, Victoria 3220, Australia.

[b]Univ. Bordeaux, CNRS, Bordeaux INP, Institut des Sciences Moléculaires, UMR 5255, 33607 Pessac, France.

[c]Department of Chemistry Giacomo Ciamician, University of Bologna, via Selmi 2, Bologna 40126, Italy.

[d]Key Laboratory of Excited-State Materials of Zhejiang Province, Institute of Analytical Chemistry, Department of Chemistry, Zhejiang University, Hangzhou 310058, China.

[e]School of Chemistry, The University of Melbourne, Parkville 3010 Victoria, Australia.

†These authors contributed equally.

*Author for correspondence.

Experimental

General Considerations

Reagents and solvents were purchased from commercial sources and used without further purification, unless otherwise stated. Ultrapure (milli-Q) water was used for all experiments. Acetonitrile was distilled over calcium hydride under a nitrogen atmosphere and collected as needed. NMR spectra were acquired on a Bruker Avance 400 spectrometer; ^{1}H NMR spectra were acquired at 400 MHz and $\{^{1}H\}^{13}C$ spectra at 101 MHz. All spectra were recorded at 298 K and chemical shifts were referenced to residual solvent peaks and quoted in terms of parts per million (ppm), relative to tetramethylsilane ($Si(CH_3)_4$). Electrospray ionization-mass spectrometry (ESI-MS) experiments were performed using a Shimadzu LCMS-9030 quadrupole time-of-flight mass spectrometer. HPLC analyses were conducted using an Agilent Technologies 1260 Infinity series equipped with quaternary pump and DAD detector. The sample (10 µL) was injected onto a Poroshell column (50 × 4.6 mm, 2.7 µm particle size) and eluted using a solvent gradient of 0%-100% acetonitrile in water over 15 min.

Synthesis of $Na_3[Ir(sppz)_3]$

The procedure was adapted from that described by Pfund *et al.*[1] for the preparation of related complexes. A mixture of sulfuric acid (27.1 mg, 0.28 mmol, 3.3 equiv.) and trifluoroacetic anhydride (2 mL) were combined in a flame dried Schlenk tube under an N_2 atmosphere. The resulting emulsion was heated to reflux with stirring until all sulfuric acid had dissolved. A deoxygenated solution of tris(phenylpyrazole)iridium(III) (51.9 mg, 0.084 mmol, 1 equiv.) in dry dichloromethane (*ca.* 17 mL) was prepared in a separate Schlenk flask.

The mixture of trifluoroacetic anhydride and sulfuric acid was transferred dropwise via cannula into the Ir(III) complex containing solution. The resulting light blue suspension was stirred overnight under N_2 at ambient temperature in the dark, during which the reaction reverted to a transparent yellow solution. To this solution, saturated aqueous $NaHCO_3$ (*ca.* 2 mL) was added. Organic solvent was removed under reduced pressure and the resulting mixture loaded onto a pre-conditioned C-18 Solid Phase Extraction Column (All-Tech, 50 mL), and eluted with H_2O. Fractions were analysed by HPLC and those containing the $Na_3[Ir(sppz)_3]$ product were collated and freeze-dried to afford an off-white/grey crystalline powder (37.9 mg, 0.041 mmol, 49% yield). ^{1}H NMR (400 MHz, CD_3OD) δ 8.41 (d, *J* = 2.70 Hz, 3H), 7.82 (s, 3H), 7.15 (dd, *J* = 7.86, 1.33 Hz, 3H), 7.05 (d, *J* = 1.87 Hz, 3H), 6.79 (d, *J* = 7.87 Hz, 3H), 6.54 (t, *J* = 2.31 Hz, 3H). ^{13}C NMR (101 MHz, CD_3OD): δ 145.6, 145.2, 139.2, 138.9, 137.9, 127.6, 124.8, 108.4, 108.6. ESI-HRMS (negative mode): *m/z* 286.331 $[C_{27}H_{18}IrN_6O_9S_3]^{3-}$ requires 286.331.

Crystallography

Single crystal X-ray diffraction data (Table S1 and Figure 1b) was collected on the MX1 beamline at the Australian Synchrotron.[2] The colourless block crystals were transferred directly from the mother liquor into immersion oil and placed under a stream of nitrogen at 100 K. Crystal structures were solved by direct methods using the program SHELXT[3] with CX-ASAP[4] and refined using a full matrix least-squares procedure based on F^2 (SHELXL),[5] within the Olex2[6] GUI program. The structure contained some disordered solvent molecules that could not be satisfactorily modelled hence the solvent mask routine within the Olex2 GUI was used.[6] A riding model was used for all hydrogen atoms.

Table S1. X-ray Crystallographic Data.

	$Na_3[Ir(sppz)_3]$
Empirical formula	$C_{75}H_{110}Ir_2N_{12}NaO_{41}S_6$
Formula weight	2435.49
Temp. (K)	100(2)
Crystal system	Trigonal
Space group	*R*-3
a (Å)	16.738(2)
b (Å)	16.738(2)
c (Å)	30.686(6)
α (°)	90
β (°)	90
γ (°)	120
Volume (Å^3)	7445(3)
Z	3
ρ_{calc} (g/cm^3)	1.630
μ (mm^{-1})	2.901
F(000)	3699
Crystal size (mm^3)	0.15 × 0.10 × 0.08
Radiation	Synchrotron λ=0.710755
2Θ range collected data (°)	3.108 to 58.07
Index ranges	$-22 \le h \le 22$, $-17 \le k \le 18$, $-36 \le l \le 36$
Reflections Collected	32851
Independent reflections	3797 [R_{int} = 0.0296, R_{sigma} = 0.0130]
Data/ restraints/ parameters	3797/1/173
Goodness-of-fit on F^2	1.046
Final R indexes [I>=2σ (I)]	R_1 = 0.0383, wR_2 = 0.1082
Final R indexes [all data]	R_1 = 0.0392, wR_2 = 0.1092
Largest diff. peak/hole (e Å^{-3})	1.54/−1.47

Spectroscopy

Measurements at ambient temperature were acquired using 10 µM metal complex in water in a quartz cuvette with a pathlength of 1 cm. Absorption measurements were obtained using a scan rate of 600 nm min^{-1} (2 nm bandwidth) on a Cary 300 Bio UV/Vis Spectrophotometer (Agilent, Australia). Photoluminescence data were acquired using a Cary Eclipse Fluorescence Spectrophotometer (600 nm min^{-1}, 5 nm bandwidth; Agilent). For low temperature measurements, the Cary Eclipse spectrophotometer was equipped with an OptistatDN Variable Temperature Liquid Nitrogen Cryostat (Oxford Instruments, UK) with a custom-built quartz sample holder.[7] Data were collected at 85 K using 5 µM metal complex solution in 4:1 spectrophotometric grade ethanol:methanol. Further cooling was not undertaken to avoid damaging the quartz sample holder.[8] Under these conditions, no significant difference in the wavelength maxima for $[Ru(bpy)_3]^{2+}$ and $Ir(ppy)_3$ was previously observed between 85 K and 77 K.[7] All photoluminescence spectra were corrected for instrumental sensitivity over the wavelength range by applying correction factors established using a quartz halogen tungsten lamp.

Electrochemistry and Electrochemiluminescence (ECL)

Electrochemical experiments were performed in a quartz electrochemical cell equipped with a glassy carbon working, platinum wire counter (CH instruments), and Ag/AgCl reference (model ET069; eDAQ Australia) electrode connected to an Autolab PGSTAT204 or Autolab PGSTAT128N potentiostat (Metrohm Australia), housed in a light-tight Faraday cage. Prior to each measurement, the working electrode was polished using 0.05 µm alumina powder and rinsed and sonicated in water; the counter electrode was rinsed with water, wiped clean, and flamed with a blowtorch; and the reference electrode was rinsed with water. ECL experiments were performed in ProCell solution (containing 180 mM TPrA as co-reactant, 0.1% surfactant and preservative in 0.3 M phosphate buffer at pH 6.8).[9] The ECL was measured by interfacing the electrochemical cell with: a photomultiplier tube (extended-range trialkali S20, ET Enterprises model 9828B) for intensity; or a charge-coupled device (CCD; QEPro, Ocean Optics) for spectral distribution.

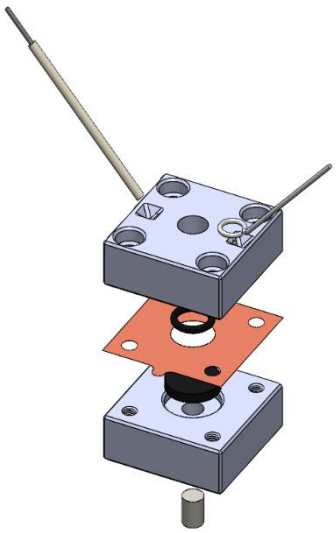

Figure S1. 3D drawing of the in-house fabricated microcell.

The calibrations shown in Figure S10 and the bead-based ECL detection depicted in Figure 4b were undertaken using a microcell (Figure S1) with a AutoLab PGSTAT128N potentiostat, inside a light-tight Faraday cage. The ECL was measured by a photomultiplier tube (model 9828B; ET Enterprises) positioned directly above the electrochemical cell. The housing of the microcell comprised two separable layers allowing for deconstruction and cleaning. The bottom layer housed a glassy carbon working electrode disc (12.7 × 2.0 mm, SKU: AU-10-008243, Microscopy Solutions) and a magnet

when required. The inner side of the top layer was lined with copper tape to allow the flow of current from a wire placed between the two pieces to the working electrode. A platinum wire counter electrode (CH Instruments) and leakless Ag/AgCl reference electrode (3.4 M KCl; model ET072; eDAQ Australia) were used. The two layers were held together by screws. Prior to each measurement, the working electrode disc was polished using 0.05 µm alumina powder and sonicated for 60 s in ethanol and rinsed with water. The Ag/AgCl reference electrode was also rinsed prior to each measurement.

Electrochemiluminescence Contour Plots

3D ECL data (intensity versus emission wavelength and applied potential) were obtained using an automated procedure created in Nova software.[10] A series of 10 s pulses of increasing potential (0.7-1.6 V *vs* Ag/AgCl at 50 mV intervals) were alternated with 10 s at 0 V *vs* Ag/AgCl. Each oxidative pulse was synchronised with the QEPro CCD detector via an HR4000 break-out box (Ocean Optics) to give ECL spectra across the potential range. Relative standard deviations for replicate experiments (n = 3) were all equal to or below 3%, calculated from the integrated emission spectrum at the applied potential giving the greatest ECL intensity. The displayed data is the average of these replicates. When the emissive enhancer was used, the ECL spectra were deconvoluted by minimising the sum of the magnitude difference between the model ($I_{total} = c_{Ru}I_{Ru} + c_{Ir}I_{Ir}$) and measured intensity (I_{meas}) at each wavelength, where c represents the metal complex concentration. Contour plots were created using OriginPro (OriginLab, USA), and ECL intensity *versus* applied potential profiles were generated by integrating the ECL spectral distribution at each applied potential.

Electrochemiluminescence Self-Interference (ECLI) Spectroscopy

The thickness of the ECL layer (TEL) of different systems was measured by ECL self-interference spectroscopy as reported previously.[11] Briefly, an indium tin oxide (ITO) layer was sputtered on a silica layer coated silicon wafer (designated as ITO/SiO_2/Si), serving as the working electrode. The ITO/SiO_2/Si electrode was fixed at the bottom of a custom-made round Teflon cell. A collimating lens was used to collect and focus the ECL signal to an optical fibre. Finally, the interferometric spectra were recorded by an optical fibre CCD-array miniature spectrometer (QEPro, Ocean Optics). A constant potential of +1.3 V was applied at the ITO/SiO_2/Si electrode for 10 s by a CHI 832C electrochemical workstation (Chenhua, China) in a three-electrode configuration, where platinum wire and Ag/AgCl (saturated KCl) served as the counter and reference electrodes, respectively. During the 10 s applied potential, ten ECL spectra with 1 s integration time were sequentially acquired. The final TEL was an average of those obtained by modelling the ECL spectra over three replicate experiments.[11] The cyclic voltammetry (CV) associated with these experiments was performed on a CHI 832C electrochemical workstation (Chenhua, China) in a three-electrode configuration, where the ITO glass, platinum wire and Ag/AgCl (saturated KCl) acted as working, counter and reference electrodes,

respectively. Synchronous acquisition of ECL intensity-voltage curves overlaid with CVs was conducted on an MPI-E ECL analytical system (Remex Instrument, China).

Electrochemiluminescence Imaging

The electrochemical cell was a three-electrode system comprising a glassy carbon (GC) working electrode, a platinum wire counter electrode, and Ag/AgCl/KCl (3 M) reference electrode. The experiments were performed using a μ-Autolab type III potentiostat. The photoluminescence and ECL images were recorded using an epifluorescence microscope from Leica (DMI6000, Leica Microsystems) and an Electron Multiplying Charge Coupled Device (EM-CCD 9100–13) camera from Hamamatsu. Photoluminescence and ECL experiments were performed in ProCell solution. We selected polystyrene beads with a diameter of 12 μm as the carrier of $[Ru(bpy)_3]^{2+}$ labels to record ECL images. The amino-functionalised beads were modified with the $[Ru(bpy)_3]^{2+}$ labels through an amide covalent bond. The bead suspension (10 μL; 2.5%) was washed with phosphate buffer (pH 7.4) and re-suspended in 1 mL of phosphate buffer. At the same time, 1 mg of $[Ru(bpy)_2(CH_3\text{-bpy-}(CH_3)_3COOH)](PF_6)_2$ was dissolved in 100 μL of dimethyl sulfoxide and this solution was added to the bead suspension. This mixture was incubated at 4°C for 3 h with continuous stirring. After incubation, the beads were washed with phosphate buffer 10 times with centrifugation for 10 min at 10,000 rpm to separate the beads from the solution. The beads were suspended in 1 mL phosphate buffer and kept at 4°C. The $[Ru(bpy)_3]^{2+}$-modified beads were deposited on a glassy carbon electrode where a constant potential was applied.

Magnetic Bead Electrochemiluminescence Assay

The $[Ru(bpy)_2(CH_3\text{-bpy-}(CH_3)_3COOH)]^{2+}$ label was converted into the *N*-hydroxysuccinimide (NHS) ester as previously described,[12] and immobilised onto amine-functionalised 1 μm magnetic beads (MagSi-NH2, MagnaMedics Diagnostics, NL). For the immobilisation process, the beads (160 μL, 10 mg/mL) were first washed 3 times with 800 μL phosphate buffer (0.1 M pH 7.2 with 0.1% Tween-20) via vortex mixing and magnetic separation. Washed beads were resuspended in 400 μL phosphate buffer, and 40 μL activated ruthenium complex label (10 mM) was added. The solution was incubated on a shaking mixer (300 rpm) overnight, shielded from light. The supernatant was then removed, and the beads were washed 4 times with the phosphate buffer to remove any unbound ruthenium complex, before being resuspended in 800 μL phosphate buffer (bead concentration: 2 μg/μL). This solution was stored in the fridge until later use. For ECL experiments, the beads solution was mixed thoroughly (vortex mixer), before 8 μg of the labelled beads were diluted with the Procell buffer solution in the microcell. A magnet was used to attract the beads to the electrode, and the ECL reaction was initiated and the emission captured with a photomultiplier tube.

Table S2. Selected spectroscopic and electrochemical properties.

	λ_{max} (r.t.)/nm	λ_{max} (85 K)/nm	$E_{0\text{-}0}$ /eV	E_{ox}/V (*vs* Ag/AgCl)	E_{red}/V (*vs* Ag/AgCl)	E_{ox}/V (*vs* $Fc^{+/0}$)	E_{red}/V (*vs* $Fc^{+/0}$)
$Ir(ppy)_3$	508 (2-MeTHF)[13], 520 (ACN)[14]	491 (2-MeTHF)[13]	2.53	0.65 (ACN)	-2.34 (ACN)	0.33 (ACN), 0.31 (DMF)[15]	-2.66 (ACN), -2.70 (DMF)[15]
$Ir(ppz)_3$		412 (2-MeTHF)[13]	3.01	0.73 (ACN)		0.40 (ACN), 0.41 (DMF)[15]	
$[Ir(sppy)_3]^{3-}$	515 (Aq.)[14]	481 (4:1 EtOH/MeOH)[14]	2.58	0.79 (Aq.), 0.81 (DMF)	-2.10 (DMF)	0.29 (DMF)[14]	-2.48 (DMF)[14]
$[Ir(sppz)_3]^{3-}$		410 (4:1 EtOH/MeOH)	3.02	0.84 (Aq.), 0.88 (DMF)		0.37 (DMF)	
$[Ru(bpy)_3]^{2+}$	621 (ACN), 625 (Aq.)[16]	580 (4:1 EtOH/MeOH)[17]	2.14	1.08 (Aq.), 1.31 (DMF)	-1.23 (DMF)	0.89 (ACN),[17] 0.81 (DMF)	-1.73 (ACN),[17] -1.73 (DMF)
$[Fe(bpy)_3]^{2+}$	~660 (^{3}MLCT, <150 fs, Aq.)[18]			0.88 (Aq.), 1.13 (DMF)	-1.23 (DMF)[i]	0.66 (ACN),[19] 0.61 (DMF)	-1.71 (ACN),[19] -1.75 (DMF)
TPrA				0.89 ± 0.06 (Aq.)[20]		0.46 (ACN/C_6H_6)[21]	
$TPrA^{\bullet}$				-1.7 (Aq.)[20]		-2.1 (ACN/ C_6H_6)[21]	

[i]Irreversible peak potential (E_p).

Figure S2. Absorbance spectra of 10 μM $[Ir(sppz)_3]^{3-}$ (blue plot) and $[Ir(sppy)_3]^{3-}$ (green plot) in water.

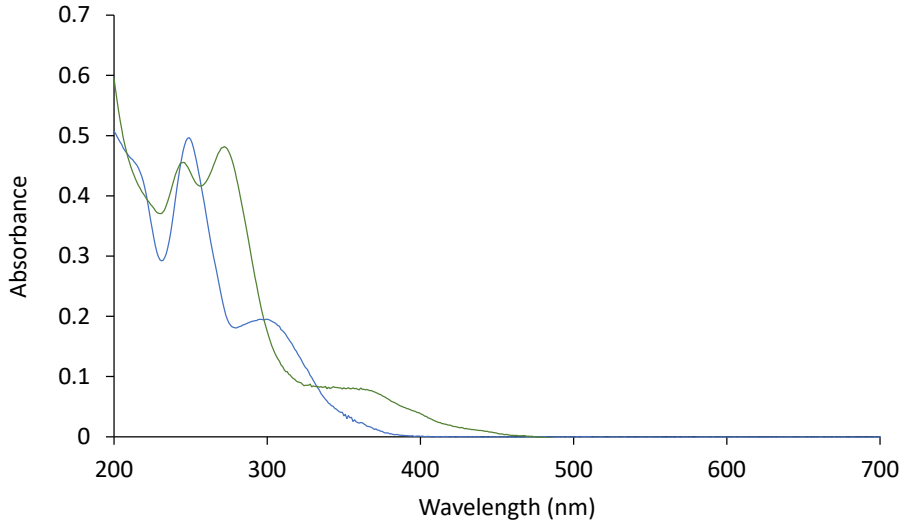

Figure S3. Low temperature (85 K) photoluminescence emission spectra of $[Ir(sppz)_3]^{3-}$ (blue plot) and $[Ir(sppy)_3]^{3-}$ (green plot), and room temperature photoluminescence emission spectrum of $[Ir(sppy)_3]^{3-}$ (dashed green plot). Conditions for low temperature spectra: 5 μM metal complex in 4:1 EtOH/MeOH, λ_{ex} = 310 nm ($[Ir(sppz)_3]^{3-}$) or 290 nm ($[Ir(sppy)_3]^{3-}$). Conditions for room temperature spectrum: 10 μM metal complex in water, λ_{ex} = 340 nm.

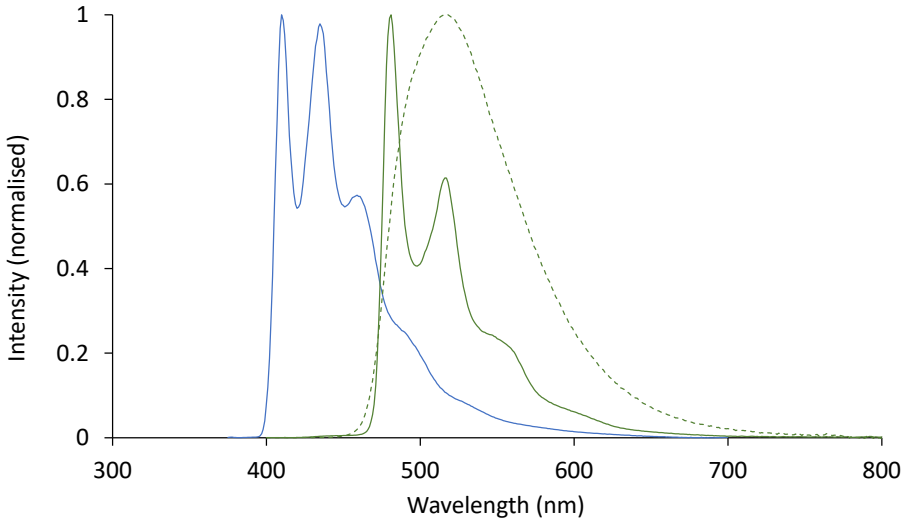

Figure S4. Cyclic voltammograms of $Ir(ppz)_3$ and $Ir(ppy)_3$ (0.2 mM) without and with an internal reference (ferrocene; 0.2 mM) in acetonitrile with 0.1 M $TBAPF_6$, after purging the solution with argon for 8 min. Scan rate: 0.1 V/s. WE: glassy carbon, CE: platinum wire, RE: Ag/AgCl.

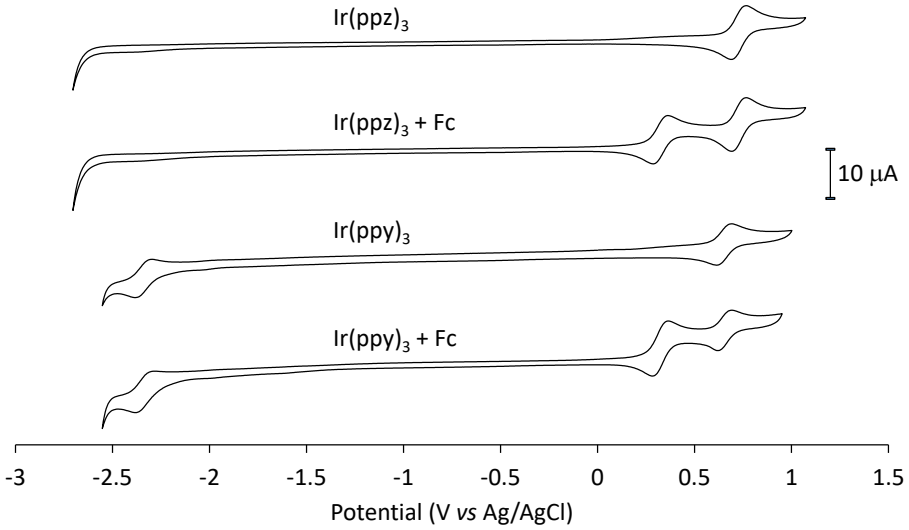

Figure S5. Cyclic voltammograms of metal complexes in phosphate buffer solution (0.1 M, pH 7.5). Scan rate: 0.1 V/s. WE: glassy carbon, CE: platinum wire, RE: Ag/AgCl.

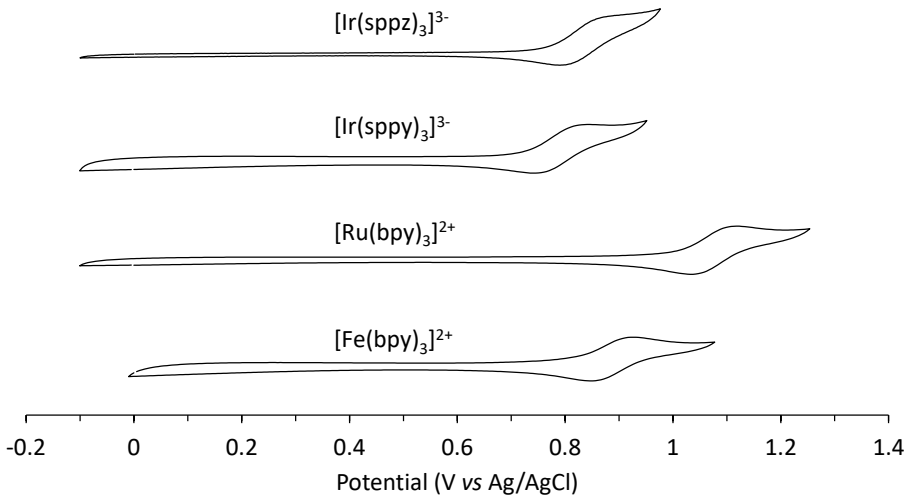

Figure S6. ECL spectra for 1 μM $[Ru(bpy)_3]^{2+}$ and either (a) $[Ir(sppy)_3]^{3-}$ or (b) $[Ir(sppz)_3]^{3-}$, in ProCell solution, using an applied potential of 0.95 V *vs* Ag/AgCl. In Fig. S6a, the black plots show the measured ECL spectra and the green and red plots show the deconvoluted emissions from $[Ir(sppy)_3]^{3-}$ and $[Ru(bpy)_3]^{2+}$. In Fig. S6b, the red plots show the measured ECL spectra, as no emission occurred from the $[Ir(sppz)_3]^{3-}$ enhancer (blue plot). Contour plots depicting the corresponding ECL spectra at applied potentials between 0.7 V and 1.6 V *vs* Ag/AgCl are shown in Fig. S7.

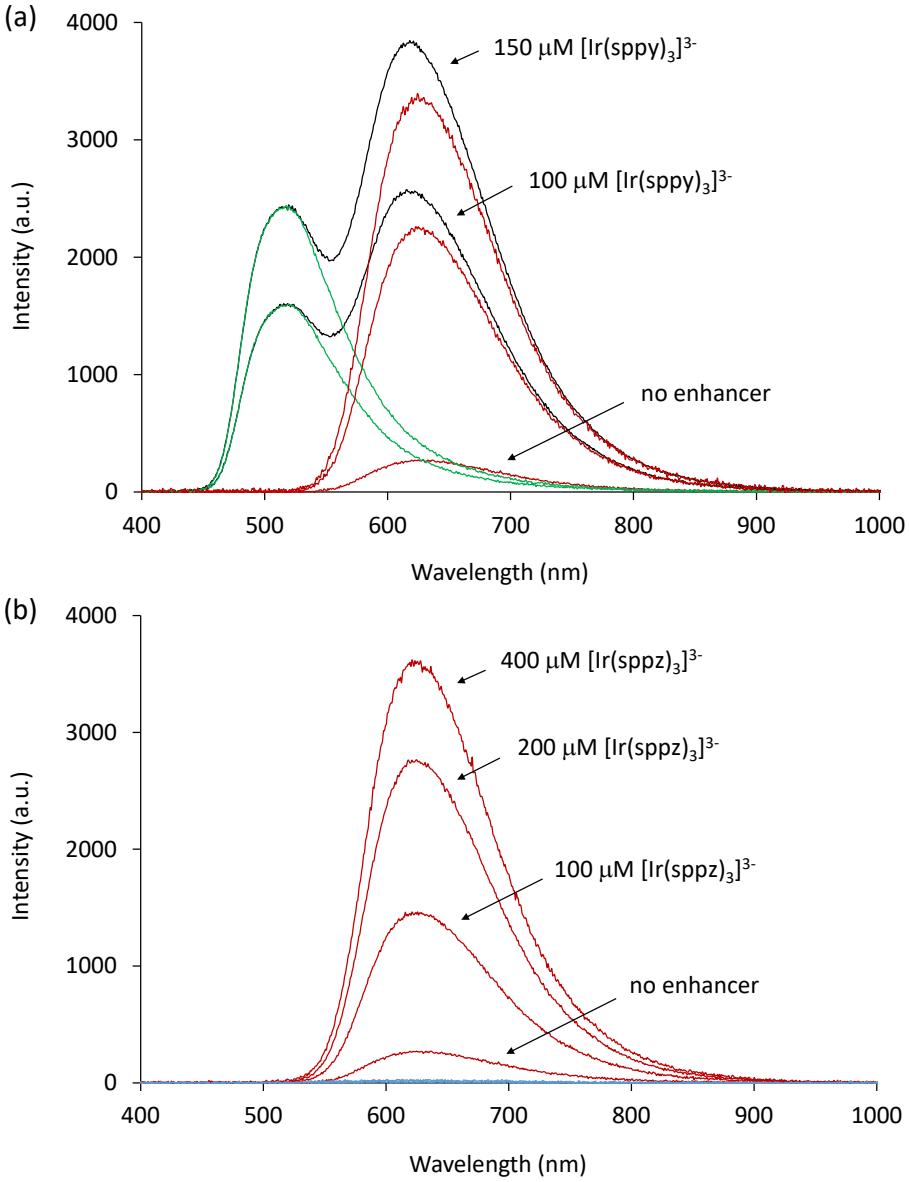

Figure S7. Contour plots of ECL *vs* wavelength and applied potential for 1 μM $[Ru(bpy)_3]^{2+}$ with: (a) no enhancer; (b) 100 μM $[Ir(sppy)_3]^{3-}$; (c) 150 μM $[Ir(sppy)_3]^{3-}$; (d) 100 μM $[Ir(sppz)_3]^{3-}$; (e) 200 μM $[Ir(sppz)_3]^{3-}$; or (f) 400 μM $[Ir(sppz)_3]^{3-}$, in ProCell solution. The plots show the ECL spectral distribution (10 s acquisition time) over a series of applied potentials (50 mV intervals), interspersed with 10 s wait times at 0 V *vs* Ag/AgCl.

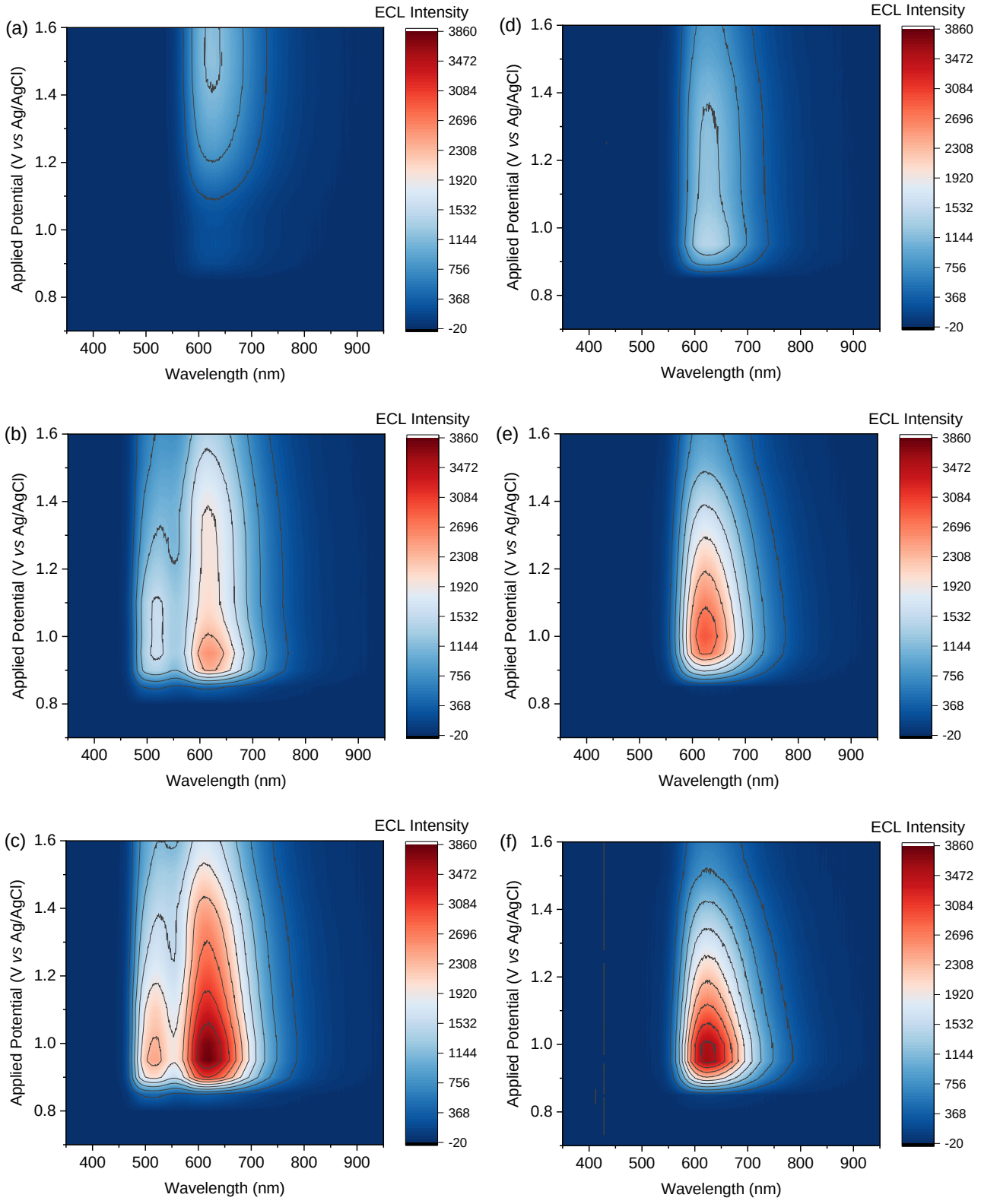

Figure S8. ECL intensity (integrated deconvoluted spectrum) of 1 μM $[Ru(bpy)_3]^{2+}$ (red plot) with either (a) 100 μM or (b) 150 μM $[Ir(sppy)_3]^{3-}$ (green plot), in comparison to the ECL intensity of 1 μM $[Ru(bpy)_3]^{2+}$ without enhancer (dashed red plot), over the applied potential range. Data was extracted from that shown in Fig. S7a-S7c.

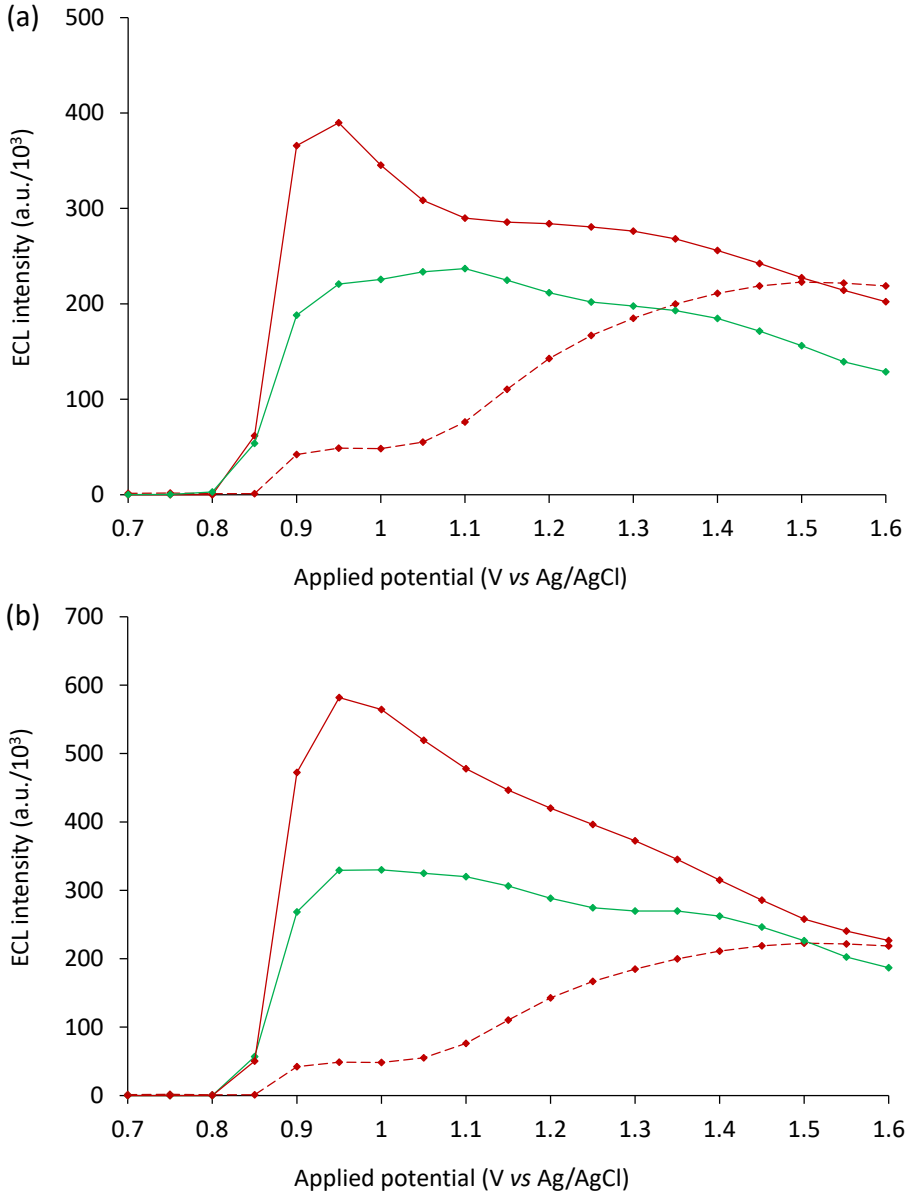

Figure S9. ECL intensity (integrated spectrum) of 1 μM $[Ru(bpy)_3]^{2+}$ (red plot) with either (a) 100 μM and 200 μM or (b) 400 μM $[Ir(sppz)_3]^{3-}$, in comparison to the ECL intensity of 1 μM $[Ru(bpy)_3]^{2+}$ with no enhancer (dashed red plot), over the applied potential range. Data was extracted from that shown in Fig. S7a, S7d-S7f.

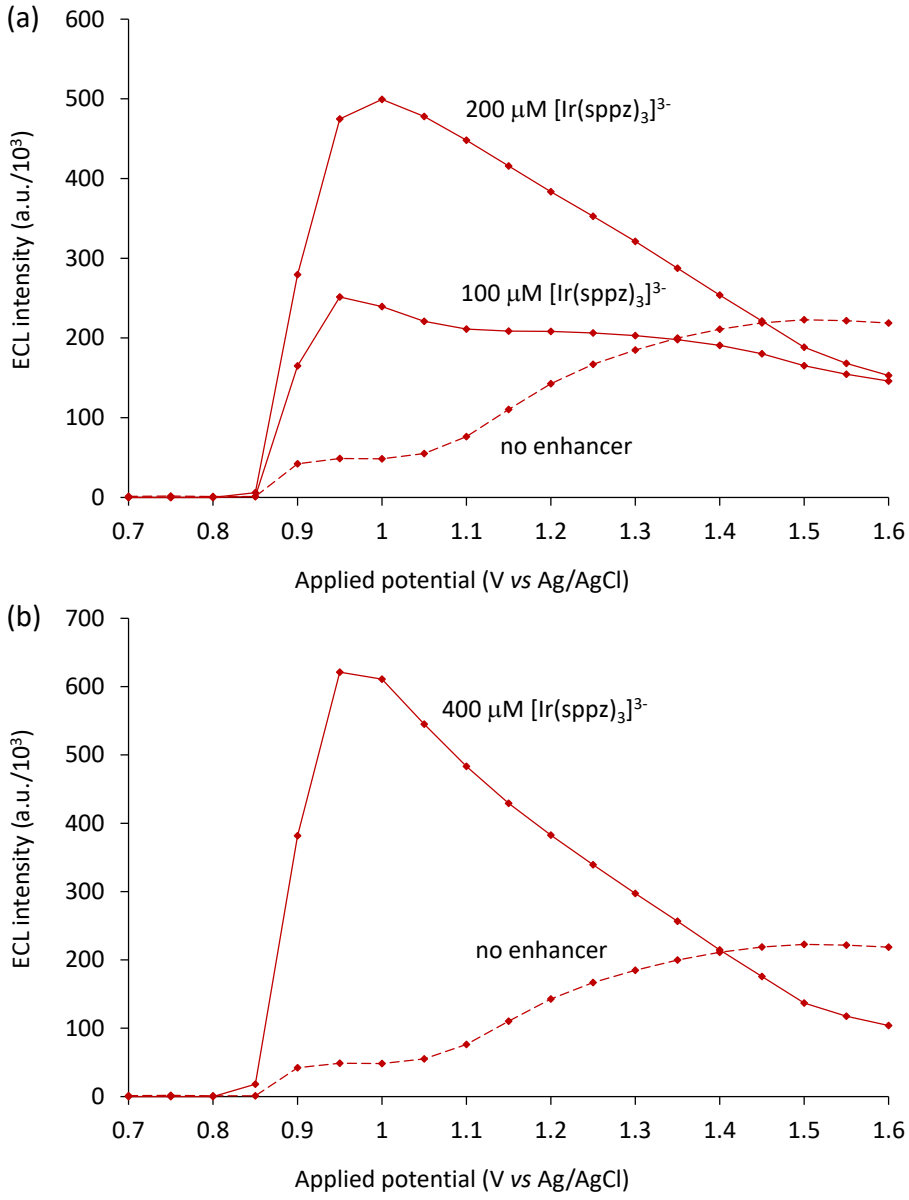

Figure S10. ECL calibration for $[Ru(bpy)_3]^{2+}$ without enhancer (blue plots) or with 200 μM $[Ir(sppz)_3]^{3-}$ (red plots) in ProCell solution, using an applied potential of (a) 1.0 V *vs* Ag/AgCl, or (b) 1.3 V *vs* Ag/AgCl. The ECL was measured using a photomultiplier tube. Each data point is an average of 3 replicates.

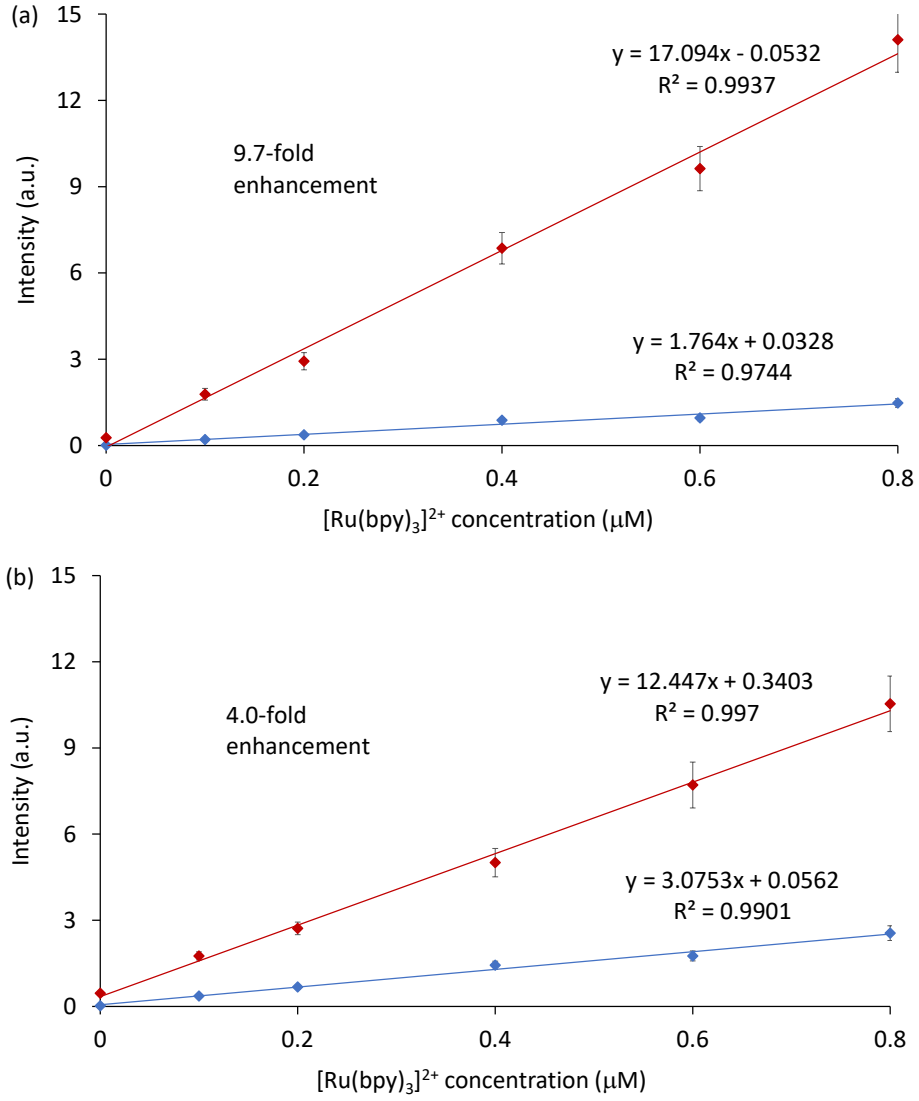

Figure S11. Contour plots of ECL *vs* wavelength and applied potential for 1 μM $[Ru(bpy)_3]^{2+}$ with (a) no redox mediator or (b) 100 μM $[Fe(bpy)_3]^{2+}$, in ProCell solution. (c) ECL intensity (integrated spectrum) of 1 μM $[Ru(bpy)_3]^{2+}$ with no redox mediator (red plot) or with 100 μM $[Fe(bpy)_3]^{2+}$ (black plot), extracted from the data shown in Fig. S11a-S11b. The contour plots show the ECL spectral distribution (10 s acquisition time) over a series of applied potentials (50 mV intervals), interspersed with 10 s wait times at 0 V *vs* Ag/AgCl.

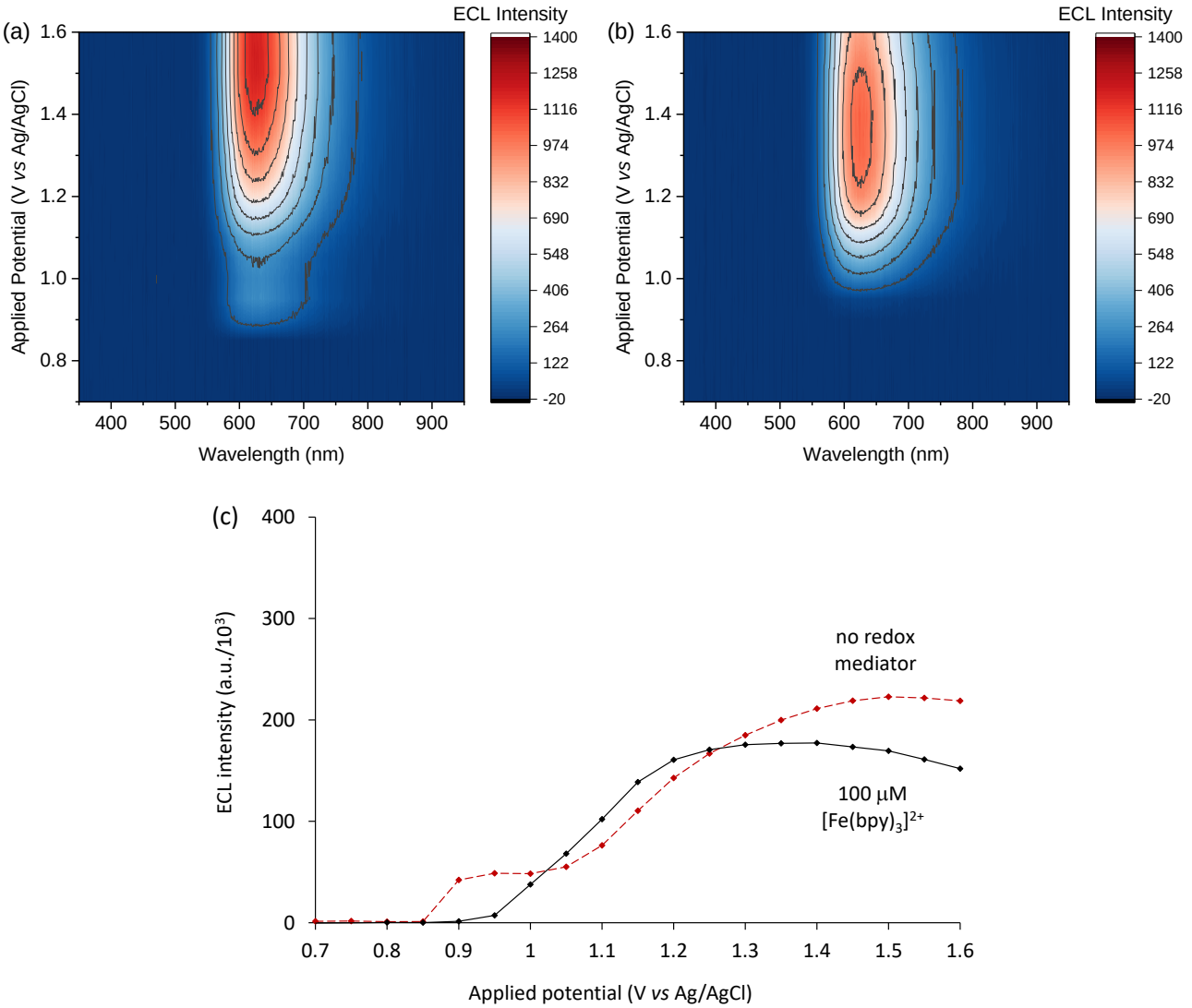

Figure S12. (a) Cyclic voltammogram of ProCell (containing 180 mM TPrA, 0.1% polidocanol, 0.3 M phosphate buffer (pH 6.8)) without (red plot) and with (black plot) 200 μM $[Ir(sppz)_3]^{3-}$, showing the increase in the rate of TPrA oxidation due to electrocatalysis by $[Ir(sppz)_3]^{3-}$. (b) The difference in the cyclic voltammograms with and without 200 μM $[Ir(sppz)_3]^{3-}$ in ProCell (blue plot; right axis), and in the same surfactant and buffer solution but without TPrA (orange plot, left axis).

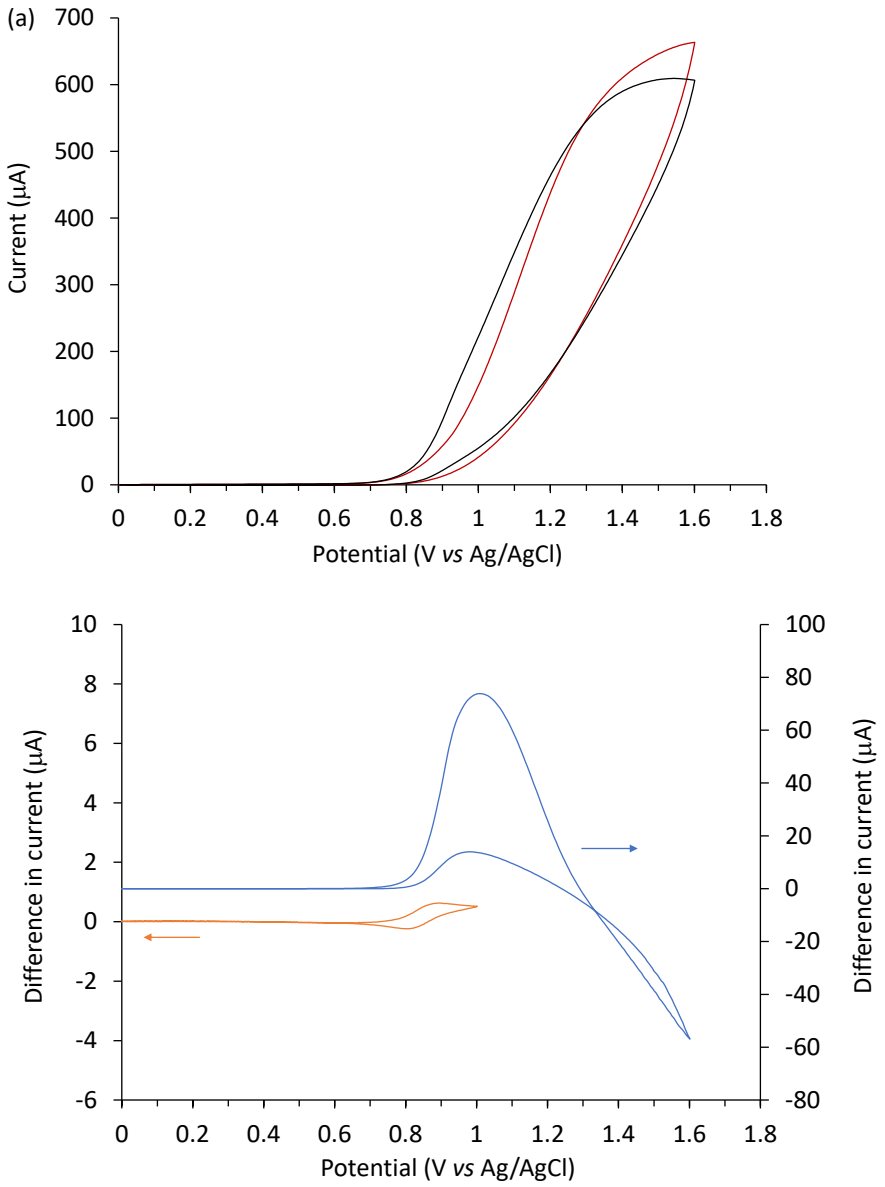

Figure S13. 'Mixed annihilation' ECL spectrum of 10 µM $[Ru(bpy)_3]^{2+}$ and 200 µM $[Ir(sppz)_3]^{3-}$ (red plot) in 4:1 acetonitrile/water containing 0.1 M $TBAPF_6$ electrolyte, where 0.1 s pulses at potentials of -1.4 V *vs* Ag/AgCl (to reduce $[Ru(bpy)_3]^{2+}$) and 0.94 V *vs* Ag/AgCl (to oxidise $[Ir(sppz)_3]^{3-}$) were alternated for 10 s. No ECL was observed when the same potentials were applied in the absence of $[Ir(sppz)_3]^{3-}$ (blue plot). Electrodes: GC working, Pt wire counter, Ag/AgCl reference.

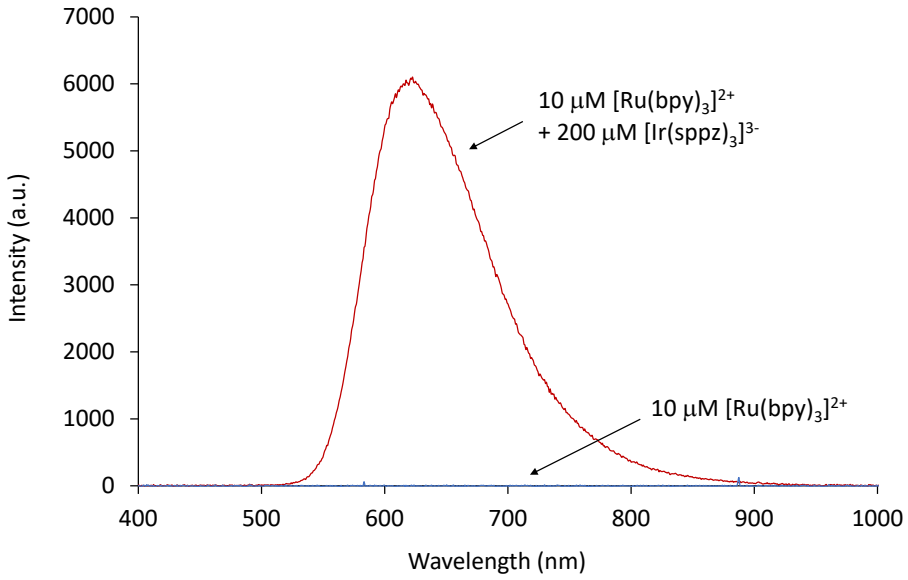

Figure S14. (a) Cyclic voltammetry using an ITO working electrode: 0.1 M phosphate buffer (black), 100 mM TPrA (grey), 10 µM $[Ru(bpy)_3]^{2+}$ (red), 0.5 mM $[Ir(sppy)_3]^{3-}$ (green), and 0.5 mM $[Ir(sppz)_3]^{3-}$ (blue). (b-f) CV (solid plots) and ECL intensity-potential curves (dashed plots) using an ITO working electrode: (b) 0.5 mM $[Ir(sppy)_3]^{3-}$, (c) 0.5 mM $[Ir(sppz)_3]^{3-}$, (d) 10 µM $[Ru(bpy)_3]^{2+}$, (e) 10 µM $[Ru(bpy)_3]^{2+}$ with 0.5 mM $[Ir(sppy)_3]^{3-}$, and (f) 10 µM $[Ru(bpy)_3]^{2+}$ with 0.5 mM $[Ir(sppz)_3]^{3-}$, dissolved in 0.1 M phosphate buffer containing 100 mM TPrA. The photomultiplier tube was biased at 250 V. The scan rate was 0.1 V s^{-1}.

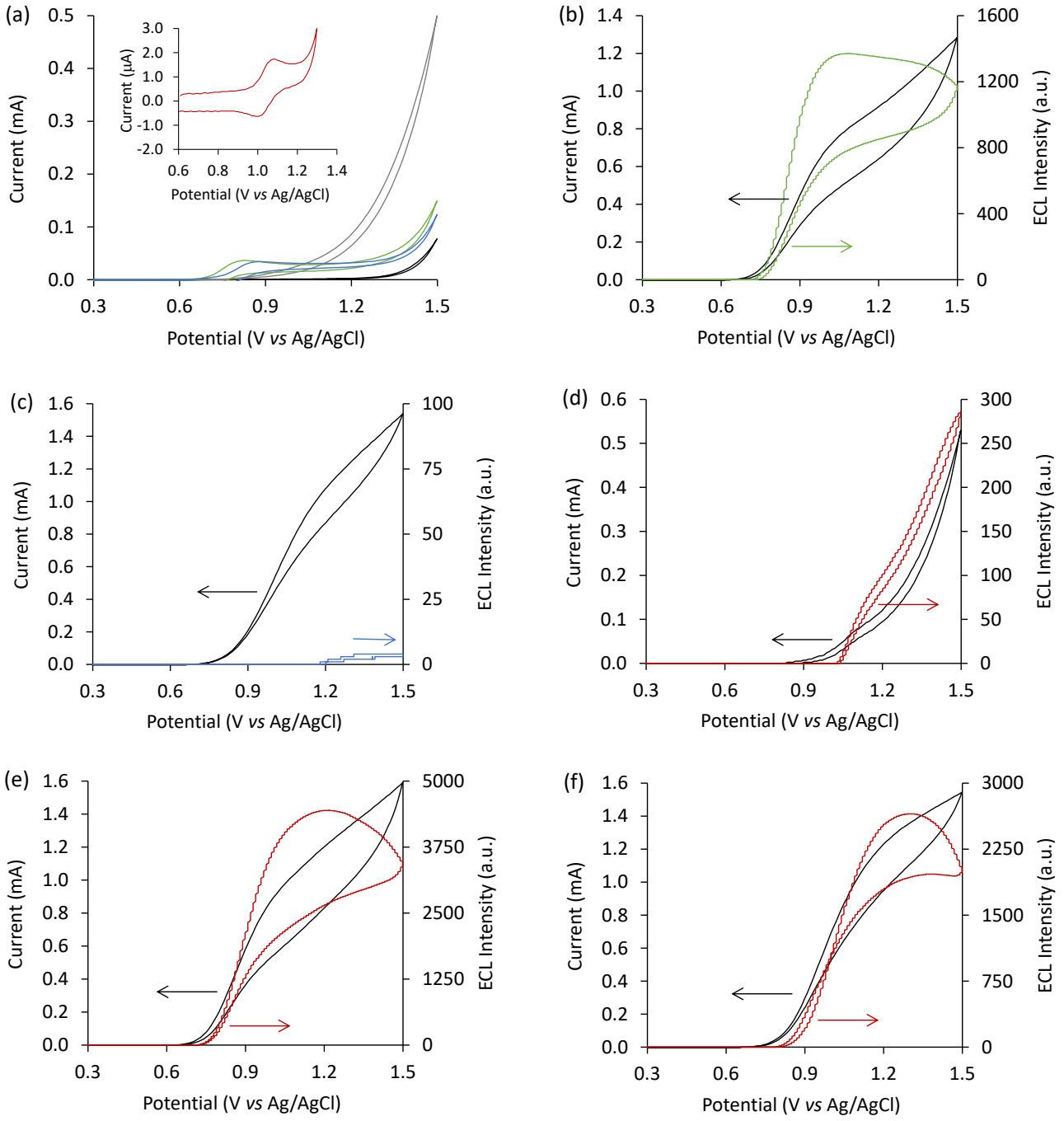

Figure S15. (a, d) Normalised ECL spectra of (a) 500 µM $[Ir(sppy)_3]^{3-}$ or (d) 500 µM $[Ru(bpy)_3]^{2+}$, in phosphate buffer (0.1 M, pH 7.4), obtained with the ITO electrode. (b, e) Normalised ECL self-interference spectra of (b) 500 µM $[Ir(sppy)_3]^{3-}$, or (e) 10 µM $[Ru(bpy)_3]^{2+}$, obtained using the ITO/SiO_2/Si electrode. (c, f) Experimental (solid curves) and simulated (open circles) ECL self-interference spectra of (c) 500 µM $[Ir(sppy)_3]^{3-}$ or (f) 10 µM $[Ru(bpy)_3]^{2+}$, obtained using the ITO/SiO_2/Si electrode. The co-reactant in all experiments is 100 mM TPrA. The constant voltage of 1.3 V (*vs* Ag/AgCl) was applied for 10 s. The spectral integration time is 1 s.

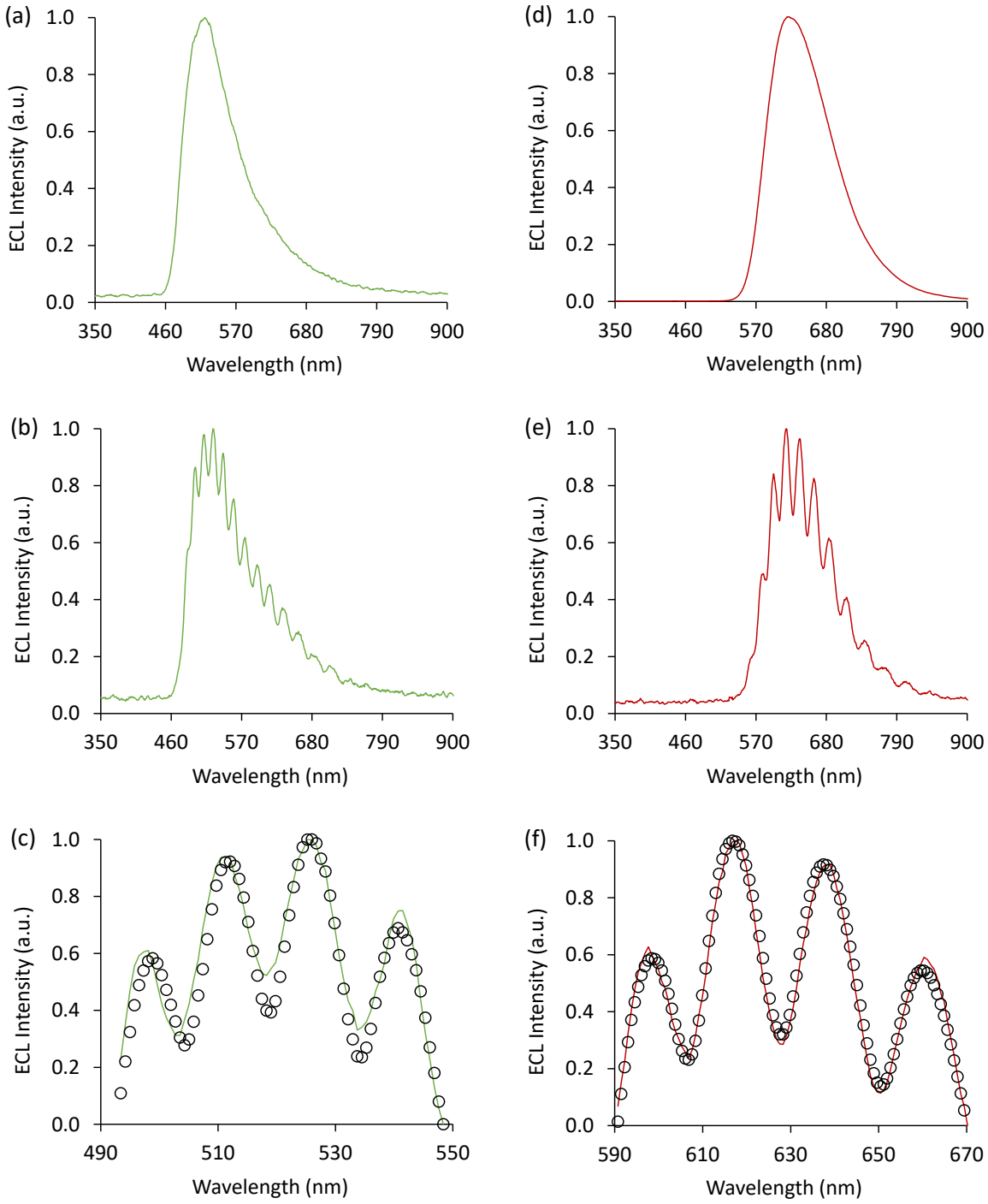

Figure S16. (a) Normalised ECL spectra for a mixture of 10 µM $[Ru(bpy)_3]^{2+}$, 500 µM $[Ir(sppy)_3]^{3-}$, and 100 mM TPrA in phosphate buffer (0.1 M, pH 7.4), obtained using the ITO electrode. (b) Normalised ECL self-interference spectra for the same solution, obtained with the ITO/SiO_2/Si electrode. (c, d) Experimental (solid curves; data from Fig. S16b) and simulated (open circles) ECL self-interference spectra of (c) the $[Ir(sppy)_3]^{3-}$ emission and (d) the $[Ru(bpy)_3]^{2+}$ emission, obtained using the ITO/SiO_2/Si electrode. The constant voltage of 1.3 V (*vs* Ag/AgCl) was applied for 10 s. The spectral integration time: 1 s.

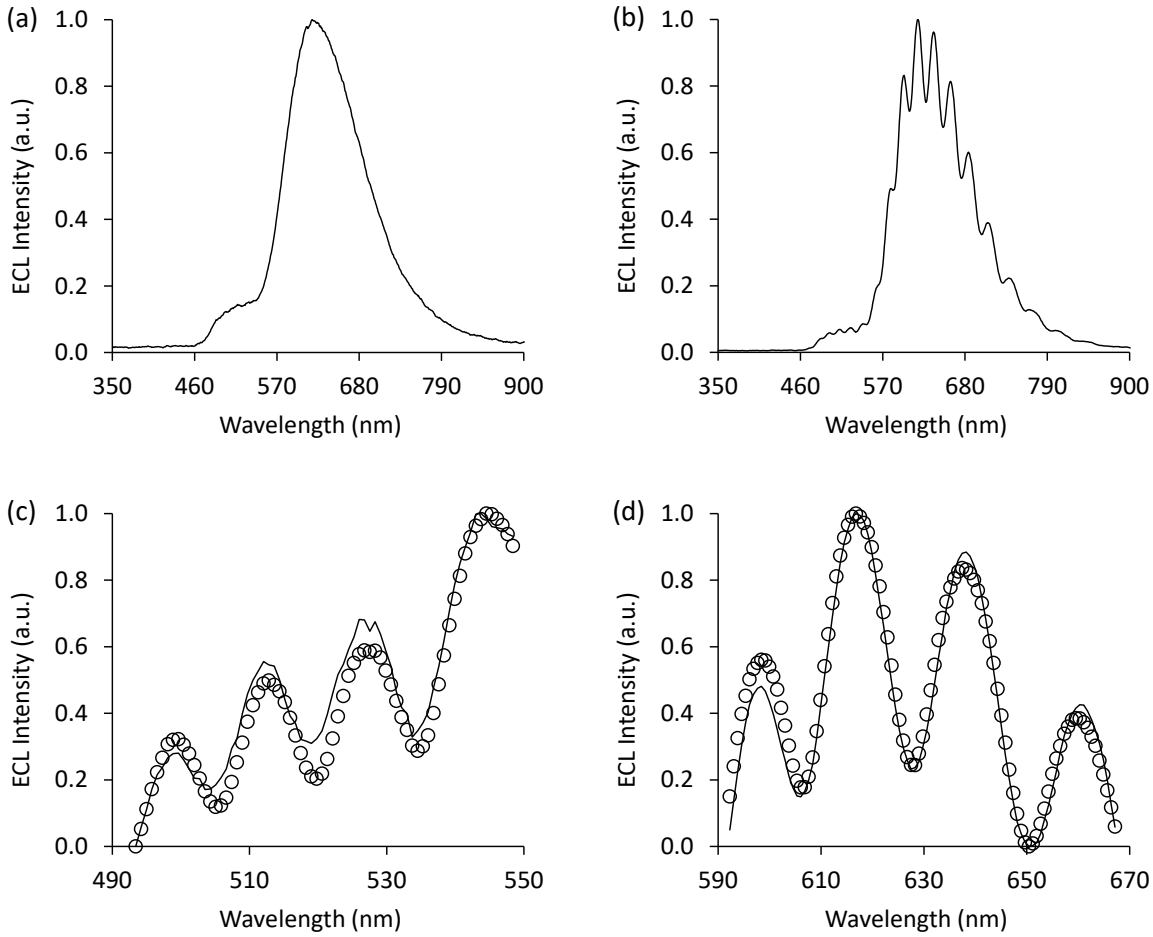

Figure S17. (a) Normalised ECL spectra for a mixture of 1 µM $[Ru(bpy)_3]^{2+}$, 500 µM $[Ir(sppy)_3]^{3-}$ and 100 mM TPrA in phosphate buffer (0.1 M, pH 7.4), obtained using the ITO electrode. (b) Normalised ECL self-interference spectra for the same solution using the ITO/SiO_2/Si electrode. (c, d) Experimental (solid curves; data from Fig. S17b) and simulated (open circles) ECL self-interference spectra of (c) the $[Ir(sppy)_3]^{3-}$ emission and (d) the $[Ru(bpy)_3]^{2+}$ emission. The constant voltage of 1.3 V (*vs* Ag/AgCl) was applied for 10 s. The spectral integration time was 1 s.

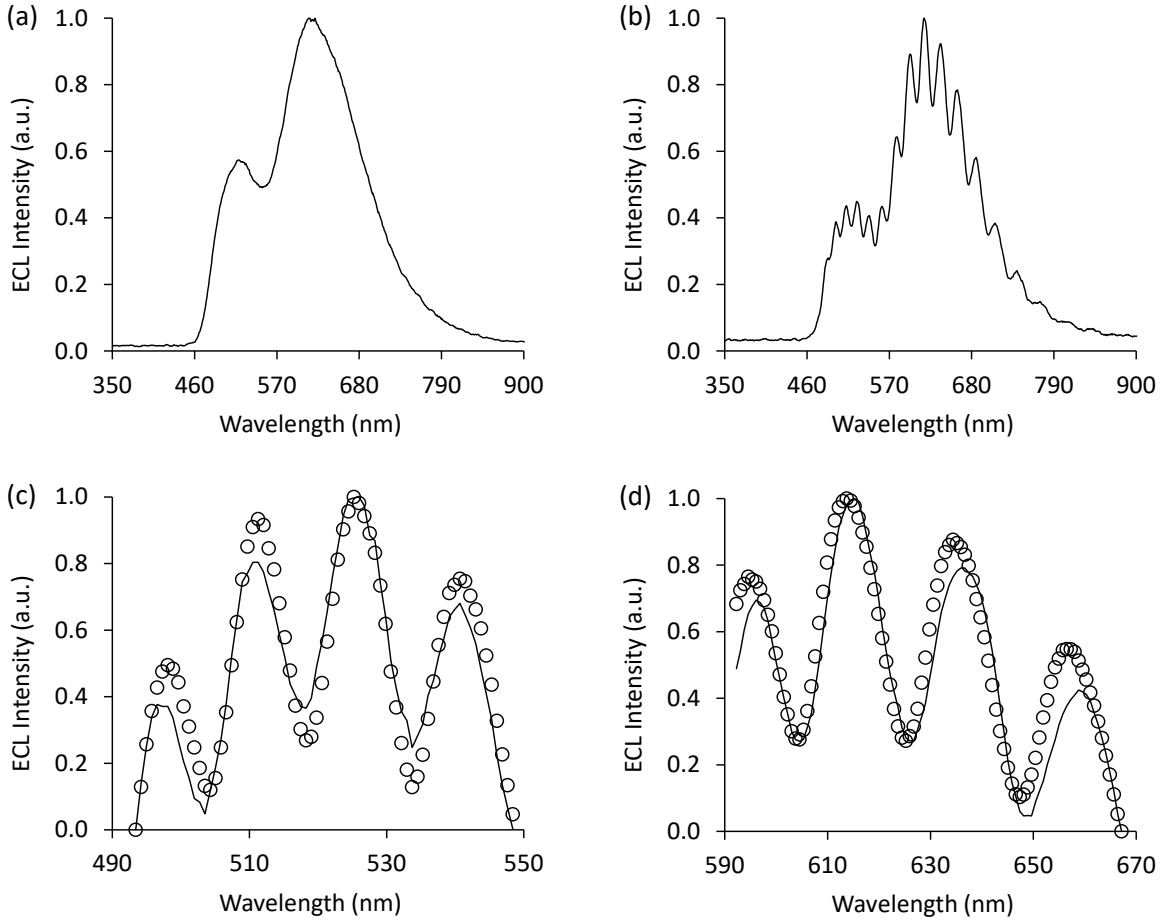

Figure S18. (a) Normalised ECL spectra for a mixture of 10 μM $[Ru(bpy)_3]^{2+}$, 500 μM $[Ir(sppz)_3]^{3-}$ and 100 mM TPrA in phosphate buffer (0.1 M, pH 7.4), obtained with the ITO electrode. (b) Normalised ECL self-interference spectra for the same solution, obtained with the ITO/SiO_2/Si electrode. (c) Experimental (solid curves, data from Fig. S18b) and simulated (open circles) ECL self-interference spectra. The constant voltage of 1.3 V (*vs* Ag/AgCl) was applied for 10 s. The spectral integration time was 1 s.

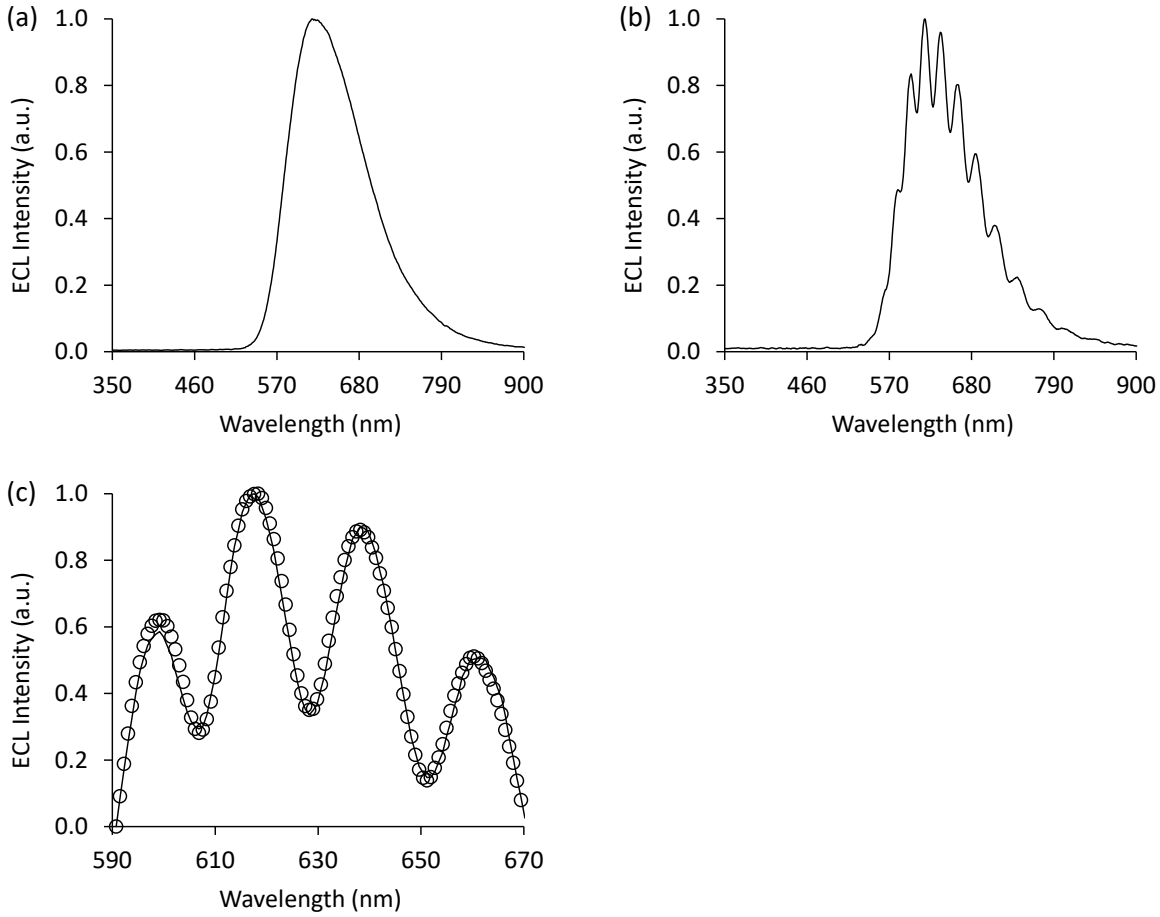

Table S3. Summary results of thickness of ECL layer (TEL) established by ECL self-interference spectroscopy.

ECL system (with 100 mM TPrA)	**TEL $[Ru(bpy)_3]^{2+}$**	**TEL $[Ir(sppy)_3]^{3-}$**
10 μM $[Ru(bpy)_3]^{2+}$	723 ± 29 nm	-
500 μM $[Ir(sppy)_3]^{3-}$	-	533 ± 84 nm
10 μM $[Ru(bpy)_3]^{2+}$ + 500 μM $[Ir(sppy)_3]^{3-}$	2431 ± 522 nm	501 ± 5 nm
1 μM $[Ru(bpy)_3]^{2+}$ + 500 μM $[Ir(sppy)_3]^{3-}$	1751 ± 218 nm	471 ± 4 nm
10 μM $[Ru(bpy)_3]^{2+}$ + 500 μM $[Ir(sppz)_3]^{3-}$	1894 ± 356 nm	-

Figure S19. ECL intensity profiles of $[Ru(bpy)_3]^{2+}$ immobilised on 12 μm polystyrene beads in ProCell solution without (solid plots) and with (dashed plots) 200 μM $[Ir(sppz)_3]^{3-}$, upon application of 1.0 V (2 s; red plots) or 1.2 V (1 s; blue plots) *vs* Ag/AgCl, measured by ECL microscopy, without background subtraction. ECL intensities were integrated over the period that the oxidative potential was applied.

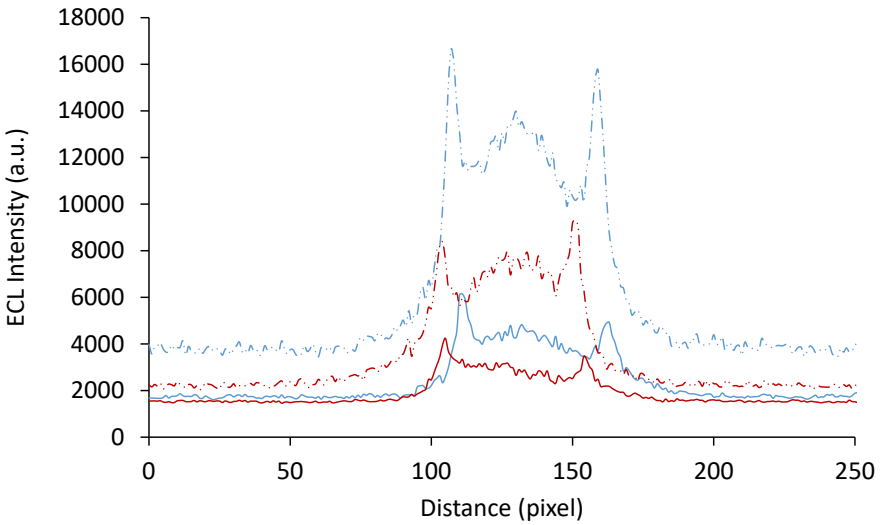

Figure S20. Relative ECL intensity (after background subtraction) of $[Ru(bpy)_3]^{2+}$ immobilised on 12 μm polystyrene beads in ProCell solution without (light columns) and with (dark columns) 200 μM $[Ir(sppz)_3]^{3-}$, upon application of 1.0 V (2 s) or 1.2 V (1 s) *vs* Ag/AgCl, measured by ECL microscopy. ECL intensities were integrated over the period that the oxidative potential was applied. Error bars represent ±1 standard deviation (n = 4). Inset photograph: ECL of single beads at an applied potential of 1.2 V without (left image) and with (right image) the enhancer.

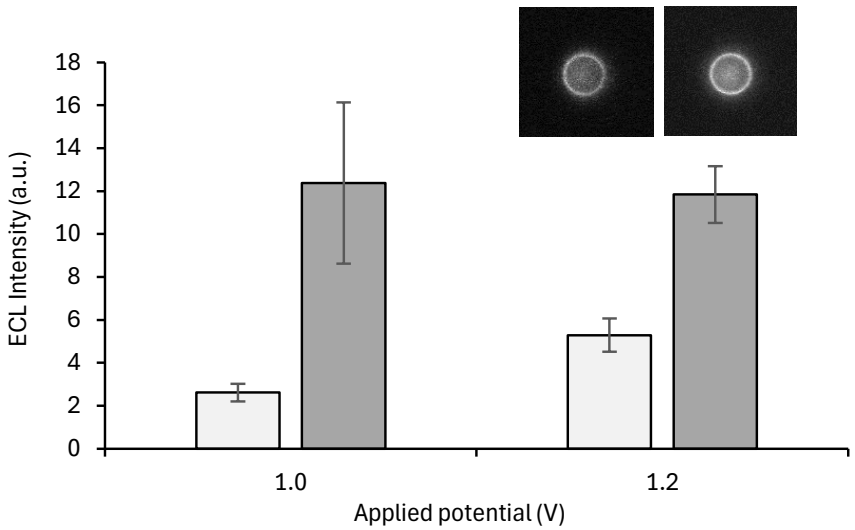

Figure S21. Relative ECL intensity (after background subtraction) of $[Ru(bpy)_3]^{2+}$ immobilised on 12 μm polystyrene beads in ProCell solution without (light column) and with (dark column) 100 μM $[Fe(bpy)_3]^{2+}$, upon application of 1.2 V (1 s) *vs* Ag/AgCl, measured by ECL microscopy. ECL intensities were integrated over the period that the oxidative potential was applied. Error bars represent ±1 standard deviation (n = 5).

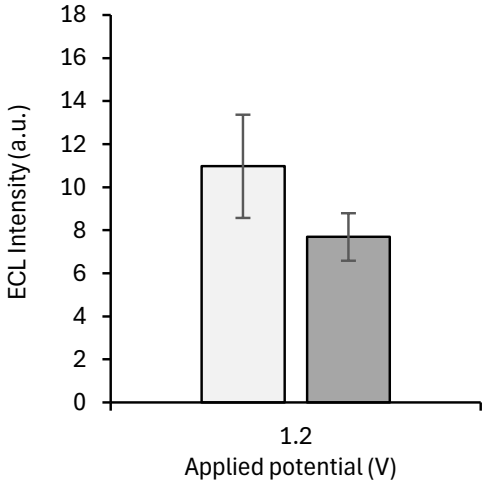

References

[1] B. Pfund, D. M. Steffen, M. R. Schreier, M.-S. Bertrams, C. Ye, K. Börjesson, O. S. Wenger, C. Kerzig, *J. Am. Chem. Soc.* **2020**, *142*, 10468-10476.

[2] N. P. Cowieson, D. Aragao, M. Clift, D. J. Ericsson, C. Gee, S. J. Harrop, N. Mudie, S. Panjikar, J. R. Price, A. Riboldi-Tunnicliffe, R. Williamson, T. Caradoc-Davies, *J. Synchrotron Rad.* **2015**, *22*, 187-190.

[3] G. M. Sheldrick, *Acta Crystallogr., Sect. A* **2015**, *71*, 3-8.

[4] A. J. Thompson, K. M. L. Smith, J. K. Clegg, J. R. Price, *J. Appl. Crystallogr.* **2023**, *56*, 558-564.

[5] G. M. Sheldrick, *Acta Crystallogr., Sect. C* **2015**, *71*, 3-8.

[6] O. V. Dolomanov, L. J. Bourhis, R. J. Gildea, J. A. K. Howard, H. Puschmann, *J. Appl. Crystallogr.* **2009**, *42*, 339-341.

[7] L. C. Soulsby, D. J. Hayne, E. H. Doeven, D. J. D. Wilson, J. Agugiaro, T. U. Connell, L. Chen, C. F. Hogan, E. Kerr, J. L. Adcock, P. S. Donnelly, J. M. White, P. S. Francis, *Phys. Chem. Chem. Phys.* **2018**, *20*, 18995-19006.

[8] C. Mallet, A. Bolduc, S. Bishop, Y. Gautier, W. G. Skene, *Phys. Chem. Chem. Phys.* **2014**, *16*, 24382-24390.

[9] E. Faatz, A. Finke, H.-P. Josel, G. Prencipe, S. Quint, M. Windfuhr, in *Analytical Electrogenerated Chemiluminescence: From Fundamentals to Bioassays* (Ed.: N. Sojic), The Royal Society of Chemistry, **2020**, pp. 443-470.

[10] S. J. Blom, N. S. Adamson, E. Kerr, E. H. Doeven, O. S. Wenger, R. S. Schaer, D. J. Hayne, F. Paolucci, N. Sojic, G. Valenti, P. S. Francis, *Electrochim. Acta* **2024**, *484*, 143957.

[11] a) Y. Wang, W. Guo, Q. Yang, B. Su, *J. Am. Chem. Soc.* **2020**, *142*, 1222-1226; b) Y. Wang, J. Ding, P. Zhou, J. Liu, Z. Qiao, K. Yu, J. Jiang, B. Su, *Angew. Chem. Int. Ed.* **2023**, *63*, e202216525.

[12] L. Chen, D. J. Hayne, E. H. Doeven, J. Agugiaro, D. J. D. Wilson, L. C. Henderson, T. U. Connell, Y. H. Nai, R. Alexander, S. Carrara, C. F. Hogan, P. S. Donnelly, P. S. Francis, *Chem. Sci.* **2019**, *10*, 8654-8667.

[13] T. Sajoto, P. I. Djurovich, A. B. Tamayo, J. Oxgaard, W. A. Goddard, M. E. Thompson, *J. Am. Chem. Soc.* **2009**, *131*, 9813-9822.

[14] E. Kerr, D. J. Hayne, L. C. Soulsby, J. C. Bawden, S. J. Blom, E. H. Doeven, L. C. Henderson, C. F. Hogan, P. S. Francis, *Chem. Sci.* **2022**, *13*, 469-477.

[15] T. Sajoto, P. I. Djurovich, A. Tamayo, M. Yousufuddin, R. Bau, M. E. Thompson, R. J. Holmes, S. R. Forrest, *Inorg. Chem.* **2005**, *44*, 7992-8003.

[16] K. Suzuki, A. Kobayashi, S. Kaneko, K. Takehira, T. Yoshihara, H. Ishida, Y. Shiina, S. Oishi, S. Tobita, *Phys. Chem. Chem. Phys.* **2009**, *11*, 9850-9860.

[17] L. Chen, E. H. Doeven, D. J. D. Wilson, E. Kerr, D. J. Hayne, C. F. Hogan, W. Yang, T. T. Pham, P. S. Francis, *ChemElectroChem* **2017**, *4*, 1797-1808.

[18] W. Gawelda, A. Cannizzo, V.-T. Pham, F. v. Mourik, C. Bressler, M. Chergui, *J. Am. Chem. Soc.* **2007**, *129*, 8199-8206.

[19] D. M. Cabral, P. C. Howlett, D. R. MacFarlane, *Electrochim. Acta* **2016**, *220*, 347-353.

[20] W. Miao, J.-P. Choi, A. J. Bard, *J. Am. Chem. Soc.* **2002**, *124*, 14478-14485.

[21] R. Y. Lai, A. J. Bard, *J. Phys. Chem. A* **2003**, *107*, 3335-3340.